Title:
Enhancement of plastic flow in lateral direction by torsional oscillation in upsetting and lateral extrusion

Authors:
Ryo Matsumoto[1,*], Sotaro Tanaka[1] and Hiroshi Utsunomiya[1]

* Correspnding author (R. Matsumoto, E-mail: ryo@mat.eng.osaka-u.ac.jp, Tel: +81-6-6879-7500, Fax: +81-6-6879-7500)

Affiliation:
[1] Division of Materials and Manufacturing Science, Osaka University, 2-1 Yamadaoka, Suita 565-0871, Japan

Abstract

Plastic flow of hollow cylinders under combining axial compression with torsion was examined in upsetting and in lateral extrusion. The hollow cylinders with initial height/outer diameter of 0.5–2.5 and initial inner/outer diameter of 0.3–0.9 were compressed/extruded and simultaneously twisted with respect to the axisymmetric forging axis in one-way or cyclic alternating. Due to superposition of torsional shear stress, the lateral metal flow was found to be assisted. Barreling of the workpiece was reduced by approximately 10% in upsetting with torsion/compression speed of 6 °/mm. The enhancement of the plastic flow in upsetting was applied to fill up tooth cavity in lateral extrusion. The extruded tooth depth of the workpiece was approximately 5–7% larger in lateral extrusion with torsion/extrusion speed of 30 °/mm. In addition, cyclic alternating torsion was effective to extrude evenly in the tooth thickness direction due to the periodic reversal of die rotation in peripheral direction.

Keywords: Forging; Torsion; Stress superposition; Plastic flow; Hollow cylinder

1. Introduction

For lightweight structural component of vehicles, forming processes of thin-walled/hollow structures or high-strength materials have strong demands in manufacturing industries (Kleiner et al., 2003). In forming of hollow components, shape defects of the components such as barreling, bending and plastic buckling are not acceptable. These defects are due to nonuniform deformation of workpiece, and mainly caused by the friction between the die and the workpiece (Osakada and Mori, 1986), inhomogeneity in the workpiece (Li et al., 2010) or plastic instability. The conventional approaches to reduce nonuniform deformation of workpiece are the lubrication and the geometry change by designing process pass chain. In other approaches, Mori et al. (2007) proposed oscillation of internal pressure to reduce plastic buckling and fracture in pulsating hydroforming of tubes. Tatematsu et al. (2018) demonstrated to fill a hollow part with oil to expand in radial direction in compression of ring workpiece.

To eliminate or shorten the post-processes, net or near-net shape forging processes have also strong demands in manufacturing industries. High forming load and severe plastic deformation are generally required in net or near-net shape forging processes such as gear forging. Since the high load tends to deteriorate the shape and dimensional accuracies of the tooth of gears, not only the reduction in forming pressure but also the control of plastic flow of workpiece are crucial technical targets. Politis et al. (2018) reviewed methods to reduce load and to control plastic flow in forging of axisymmetric shapes. In gear forging, Ohga and Kondo (1982) proposed the divided flow method to control plastic flow under low forming pressure. Weiss et al. (2018) proposed a preforming method to fill tooth cavity in face gear forming under low forming pressure. Osakada et al. (1997) proposed a die forging method with an axially driven die to fill the corners of the die cavity under low forming pressure. Ando (2015) reported the effects of ram speed control for temperature change of workpiece

on the dimensional accuracy of the tooth of gear in cold forging with a servo press.

One of major approaches to control plastic flow in metal forming processes is the multi-axial deformation. It is well known that plastic deformation of workpiece is promoted through the superposition of axial and shear stresses in the theory of plasticity (Bridgman, 1943). Tekkaya et al. (2015) reviewed the applications of stress superposition in metal forming processes. Practical stress superposition in axisymmetrical forging process is the combination of axial and peripheral die movements. The multi-axial deformation is easily realized by combining with torsion with respect to the axisymmetric forging axis.

Some research works concerning plastic flow and microstructure evolution in forging with torsion were already reported. Especially KOBO type forming process (Bochniak and Korbel, 2003) is a well-established forging process with torsion. Bochniak et al. (2006) investigated the microstructure evolution in KOBO type forming of hot gear forging. Weglarczyk et al. (2008) reported the plastic flow in gear-wheel forging with reversible rotation die by the finite element simulation. Maciejewski et al. (2008) theoretically predicted the dead zone and the radial flow in forward extrusion with cyclic torsion by an upper bound analysis. Korbel et al. (2011) observed the microstructure after forward extrusion with cyclic torsion. Koprowski et al. (2018) investigated the influence of the oscillation frequency on the microstructure and mechanical properties in forward extrusion with cyclic torsion.

In forming processes other than KOBO type forming, Kim and Park (2003) proposed the velocity distribution over workpiece for an upper bound analysis and numerically predicted the strain distribution for the finite element simulation in the backward extrusion with torsion. Wang et al. (2017) reported the strain distribution in backward extrusion with peripheral torsion by the finite element simulation. Since torsion with respect to the axisymmetric forging axis changes the direction of the plastic flow of the workpiece and induces plastic strain additionally to the workpiece, large metal flow and grain refinement of

the workpiece were realized in above research works. Furthermore, many of these were investigated by combination of compression and torsion without changing the shape of the workpiece, such as high-pressure torsion (HPT) test (Bridgman, 1964) and other test (Saunders and Nutting, 1984). In recent years, dynamic high-pressure torsion test (Verleysen and Lanjewar, 2020) and circumferential twisting in equal-channel angular pressing (ECAP) (Lee et al., 2018) were developed as severe plastic deformation (SPD) processing with torsion. On the other hand, the deformation change of the workpiece in forging processes with torsion is not sufficiently understood. It is supposed that the plastic flow in the lateral direction is assisted by combining axial deformation with torsion because the combined axial and the peripheral loads increases in the cross-section of the workpiece in forging processes with torsion.

In order to enhance plastic flow in the lateral direction, in this study, torsion with respect to the axisymmetric forging axis is simultaneously combined with the axial deformation in upsetting of hollow cylindrical workpiece. The influence of torsional oscillation on the barreling of the workpiece is investigated by the experiment and the finite element analysis. The results of upsetting with torsional oscillation are applied to fill the workpiece into the tooth cavity in lateral extrusion with gear shape.

2. Theoretical relationships

2.1. Relationship between axial stress and torsion speed

On the assumption of isotropic deformation without work hardening, axial stress in the z direction (σ_z) and shear stress with respect to the z-axis ($\tau_{z\theta}$) are simultaneously combined. The relationship between σ_z and the plastic strain increments in the z direction ($d\varepsilon_z^p$) and with respect to the z-axis ($d\varepsilon_{z\theta}^p = d\gamma_{z\theta}^p/2$) is given by the Lévy-Mises equations as follows:

$$\sigma_z = 3\tau_{z\theta}\frac{d\varepsilon_z^p}{d\gamma_{z\theta}^p} \tag{1}$$

On the other hand, the Mises yield criterion is described as follows:

$$Y^2 = \bar{\sigma}^2 = \sigma_z^2 + 3\tau_{z\theta}^2 \tag{2}$$

where Y and $\bar{\sigma}$ are the uniaxial yield stress and the equivalent stress, respectively. From **Eqs. (1) and (2)**, the relationship between σ_z and $d\gamma_{z\theta}^p/d\varepsilon_z^p$ is described as follows:

$$\sigma_z^2 = \frac{3\bar{\sigma}^2}{\left(d\gamma_{z\theta}^p/d\varepsilon_z^p\right)^2+3} \tag{3}$$

Eq. (3) means the axial stress decreases with increasing the shear stress. When the compression speed in the z direction, torsion speed with respect to the z-axis and radial distance from the z-axis are given as v, ω and r, respectively, **Eq. (3)** is described as follows:

$$\sigma_z^2 = \frac{3\bar{\sigma}^2}{(r\omega/v)^2+3} \tag{4}$$

Figure 1 shows the relationship between σ_z/σ_{z0} and $r\omega/v$ in **Eq. (4)**. Here σ_{z0} is the axial stress in the z direction at $\omega = 0$. In upsetting with torsion, axial load in the z direction is predicted to decrease with increasing torsion speed with respect to z-axis.

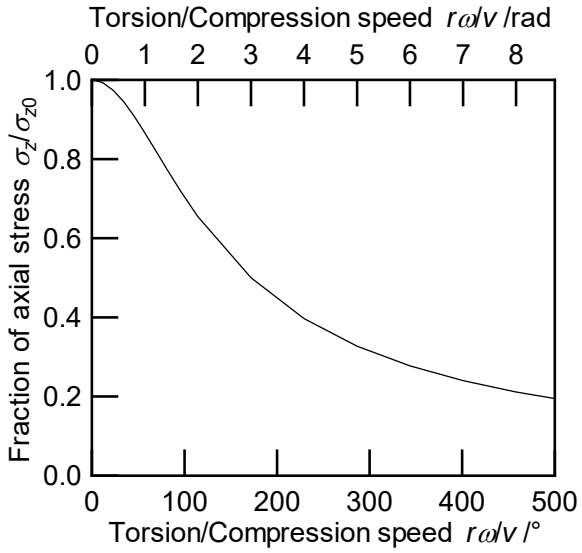

Fig. 1 Theoretical relationship between fraction of axial stress and torsion/compression speed in compression of cylindrical material with isotropic deformation without work hardening.

2.2. Theoretical relationship between torque and shear stress

When the hollow cylinder with no hardening was plastically twisted without changing the height and the shape of the cross-section in the peripheral (θ) direction with respect to z-axis, the average shear stress (τ) in rθ cross-section is derived as follows (Nadai, 1950):

$$\tau = \frac{4}{\pi(D+d)^3}\left(\theta\frac{dT}{d\theta} + 3T\right) \quad (5)$$

where T, θ, D and d are the torque, torsion angle, outer and inner diameters of cylinder, respectively. Here the average shear stress is estimated at the center of the wall thickness of the cylinder. In upsetting of hollow cylindrical workpiece with torsion, the shear stress is confirmed to be combined by the torque.

3. Experimental conditions

3.1. Workpiece and die materials

JIS A1070 aluminum drawn bars were used as initial materials for upsetting and lateral extrusion. It was selected according to the maximum capacities of load (100 kN) and torque (200 N·m) of forging machine (Matsumoto et al., 2017) used in this study. An initial material was machined to cylindrical shape with D_0 = 10.0 mm in outer diameter, d_0 = 3.0–9.0 mm (standard condition: 5.0 mm) in inner diameter and h_0 = 5.0–25.0 mm (standard condition: 15.0 mm) in height for upsetting. Another initial material was machined to cylindrical shape with D_0 = 9.5 mm in outer diameter, d_0 = 3.0 mm in inner diameter and h_0 = 13.4 mm in height for lateral extrusion. The surface roughness of the hollow cylindrical workpiece was Ra = 1.0 μm on the outer surface, 4.2 μm on the inner surface and 0.30–0.50 μm on end surfaces.

Dies for the upsetting and the lateral extrusion were made of JIS SKH51 high-speed

tool steel (63 HRC). The contacting surfaces on the dies to the workpiece were polished to mirror-like finish (Ra = 0.02–0.03 μm). The upsetting and the lateral extrusion were conducted without lubrication at room temperature.

3.2. Upsetting

The hollow cylindrical workpiece was placed between two parallel flat platens with mirror-finished end surface as illustrated in **Figure 2**. The workpiece was compressed in height by the upper die at an axial speed of v = 0.1 mm/s. The lower die started to rotate immediately after axial compression load reached 5 kN (reduction in height $\Delta h/h_0$ = 5%). The workpiece was twisted with respect to the axisymmetric compression axis in one-way or cyclic alternating (amplitude a = 5° (π/36 rad)) at peripheral speed of ω_r = 0–0.5 rpm (0–0.05 rad/s) by the frictional force between the lower die and the workpiece. The maximum frequency of cyclic alternating torsion was 0.15 Hz.

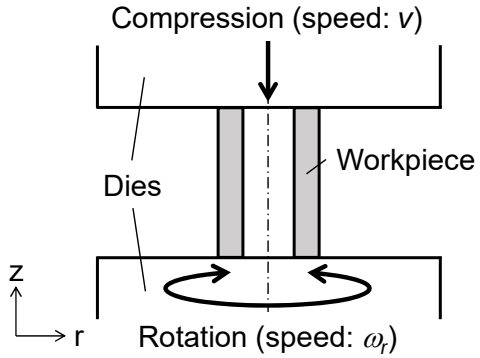

Fig. 2 Schematic illustration of upsetting with torsional oscillation of hollow cylindrical workpiece with parallel flat platens.

3.3. Lateral extrusion with gear shape

Figure 3 shows the die arrangement and the tooth geometry of the die for lateral extrusion with gear shape. A regular hexagonal concave with side length of 5.6 mm and a

depth of 3.0 mm was prepared at the center of the tip of the punch. Total of eight grooves with a tooth thickness of 3.0 mm, a tooth width of 3.0 mm, and a tooth depth of 15.0 mm were prepared at every 45° in the peripheral direction of the die. The grooves were imitated the tooth profile of gear, however the grooves were designed enough deep for the workpiece to fill up the tip of the grooves during extrusion. For prevention of excessive extrusion pressure, a relief hole with a diameter of 1.0 mm and a depth of 5.0 mm was prepared at the center of the die. The die and the container were fixed with bolts so that no sliding was allowed between the die and the container.

The punch was moved down with v = 0.1 mm/s, while the container and die were rotated with respect to the axisymmetric extrusion axis in one-way or cyclic alternating (a = 5° (π/36 rad)) at ω_r = 0.5 rpm (0.05 rad/s). The workpiece was twisted by the engagements among the extruded workpiece and the concave of the punch and the groove of the rotated die.

Figure 4 shows the deformation behavior of the workpiece in lateral extrusion. The deformation behavior was predicted by the finite element analysis. In each figure, the left and right halves show the appearance and sectional view, respectively. The upper end and side surfaces of the workpiece started to be plastically flown into the concave of the punch and the grooves of the die at the punch stroke s = 0.7 mm, respectively. Then the concave of the punch was filled with the workpiece at s = 4.8 mm, and the workpiece was laterally extruded in inner and outer radial directions into the die. The hole of the workpiece was shrinked near the bottom at s = 6.7 mm, then the bottom center of the workpiece started to be plastically flown into the hole with a diameter of 1.0 mm at the bottom of the die.

Based on the predicted deformation behavior of the workpiece, both the container and the die started to rotate at s = 0.7 mm, and the cumulative rotation angle was set to 180° (π rad) at s = 6.7 mm in experiment. The aim of the die rotation is to enhance the plastic flow of the workpiece to the grooves of the die.

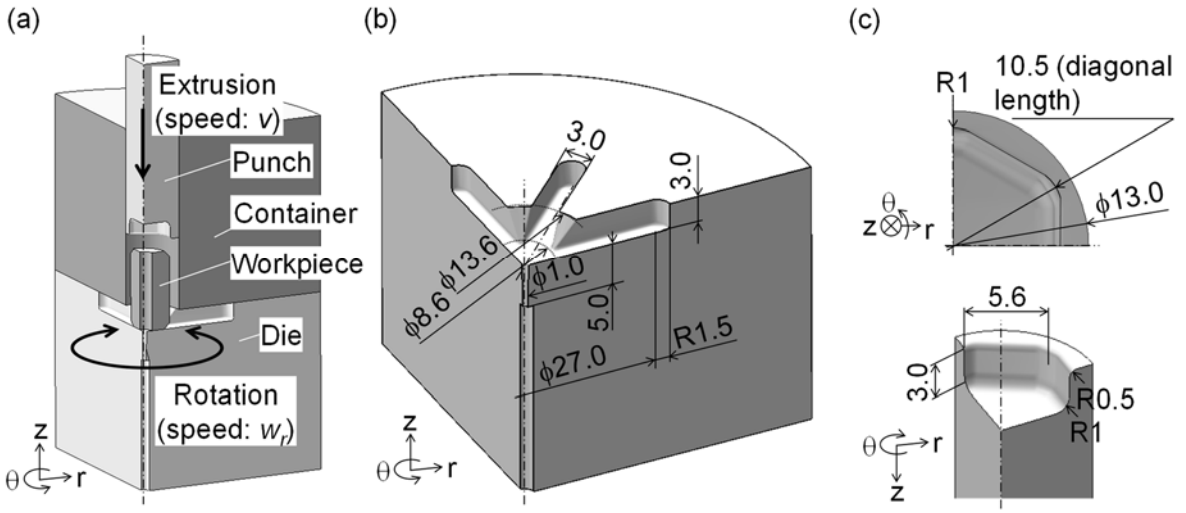

Fig. 3 (a) die arrangement, (b) shape of tooth part of die and (c) end shape of punch for lateral extrusion with gear shape.

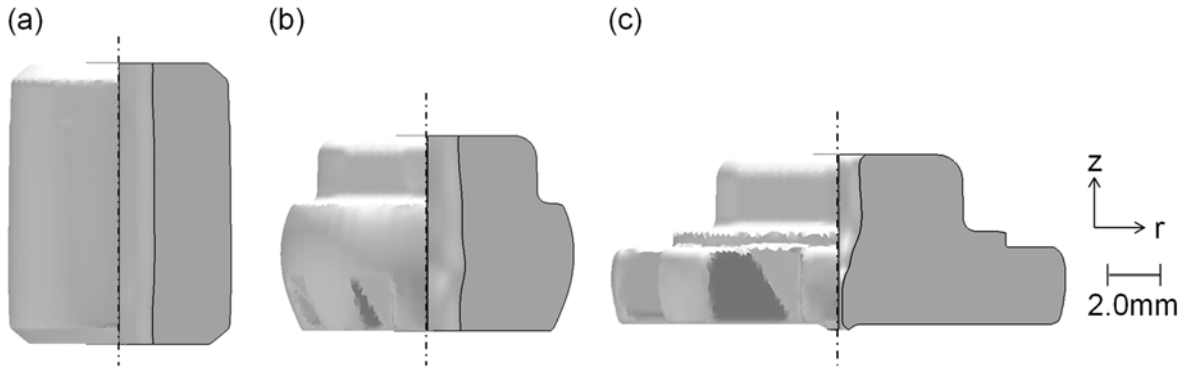

Fig. 4 Deformation behavior of hollow cylindrical workpiece in lateral extrusion with gear shape (left half: appearance, right half: section, finite element analysis): (a) axial stroke s = 0.7 mm, (b) s = 4.8 mm, (c) s = 6.7 mm.

4. Finite element analysis conditions

In parallel with the forging experiments, the finite element analysis was carried out by using a commercial three-dimensional finite element code, Simufact Forming ver. 15.0 (MSC Software Company). In the analysis, the elastic-plastic finite element method for

deformation and the heat conduction finite element method for temperature change were applied to calculate the stress, strain, and temperature of the workpiece. Crack initiation and microstructural change in the workpiece were not considered in the analysis.

In this study, the element type of the workpiece was a hexahedral 8-node element with 0.35 mm and 0.20 mm on a side in upsetting and lateral extrusion, respectively. When the element strain was cumulated larger than 0.4, the elements were automatically remeshed to hexahedral 8-node elements. The workpiece was assumed to be a pure aluminum for industrial use, while the dies were treated as rigid bodies with isothermal state. The material properties of the aluminum workpiece were employed from the built-in database of material properties in Simufact Forming ver. 15.0. The model of the flow stress was isotropic hardening, and the dependences of temperature and strain rate sensitivity on the flow stress were also taken into account. The temperature dependences of the Young's modulus, the thermal conductivity, and the specific heat were taken into account. The detailed material properties used for the analysis were shown in our previous research work concerning upsetting with torsional oscillation (Matsumoto et al., 2017). The Coulomb's friction law was adopted because the law was used widely in the finite element analysis of cold forging process. In addition, the frictional force and the deformation may be influenced by the change in the forming pressure because the forming pressure was reduced by combining with torsion in upsetting. On assumption of the Coulomb's friction law, the coefficient of friction was set μ = 0.1 on the die–workpiece interface. The coefficient of friction was determined to be agreed with the relationship between the rotation angle of the lower die and the twisted angle of the workpiece in the experiment (the circle marks plotted in **Figure 5(a)**) and the finite element analysis under various coefficients of friction. From our previous research work (Matsumoto et al., 2017), the heat transfer coefficients on the die–workpiece interface and the free surfaces of the workpiece were assumed to be 5000 W/(m^2·K) and 50 W/(m^2·K), respectively.

5. Upsetting of hollow cylinder

5.1. Axial load and torque

Figure 5 shows the experimental results of the rotation angle of the lower die, the torque and the axial load in upsetting with ω_r = 0.5 rpm. Here three solid lines are the rotation angle of the lower die in each torsions, while the dashed line with plotted circle marks are twisted angle of the workpiece in one-way torsion. The workpiece was peripherally twisted by means of the peripheral rotation of the lower die because the torque increased immediately after the die rotation started at $\Delta h/h_0$ = 5%. The torque dropped periodically and momentarily in cyclic alternating rotation of the lower die because the actual rotation of the workpiece stopped at the moments of reversal of the die rotation direction. The average shear stress in upsetting with ω_r = 0.5 rpm is shown in **Figure 6**. Here the average shear stress was estimated by **Eq. (5)** using the torque in **Figure 5(b)**. The average diameters before and after upsetting were used. The shear stress is confirmed to be combined by the torque in upsetting with torsion.

Since the workpiece was peripherally twisted by the frictional force between the die and the workpiece in upsetting with flat smooth dies as mentioned in Section 3.2, the peripheral slip may occur on the die–workpiece interface. The twisted angle of the workpiece in the one-way torsion was plotted with circle mark in **Figure 5(a)**. Here the twisted angle of the workpiece was characterized as the peripheral angle between the two lines scribed on the upper and lower end surfaces of the workpiece. The twisted angle of the workpiece was approximately one-tenth of the rotation angle of the lower die. The torsion speed (ω_t) estimated from the twisted angle and duration was approximately 0.1 rpm (ω_t/v = 6 °/mm).

The axial load was reduced by approximately 10% at immediately after the die rotation started in cyclic alternating rotation in **Figure 5(c)**. On the other hand, the axial load

was slightly reduced in one-way torsion at $\Delta h/h_0 < 30\%$ because the torque in one-way torsion was lower than that in cyclic alternating torsion at $\Delta h/h_0 < 30\%$. However, maximum reduction in the axial load was almost the same in one-way and cyclic alternating torsions. This may be because peripheral slip on die–workpiece interface in one-way torsion was larger than that in cyclic alternating torsion at $\Delta h/h_0 < 30\%$. The reduction in axial load is due to superposition of the axial compression and torsion stresses. When the experimental conditions of upsetting with ω_t/v = 6 °/mm was applied to **Eq. (4)**, the value of $r\omega/v$ was estimated approximately 25–30°. Here the effective radius (Barraclough et al., 1973) was used as approximately 0.8r for $d_0/D_0 = 0.5$. Therefore the axial load was theoretically predicted to be reduced by approximately 5–10% from **Figure 1**. In addition, the axial load was experimentally reduced by approximately 7% and 14% with ω_t/v = 6 °/mm and 15 °/mm in upsetting with grooved dies, respectively (Matsumoto et al., 2017). Hence 10% reduction in axial load in **Figure 5(c)** is reasonable for the torsion/axial speed.

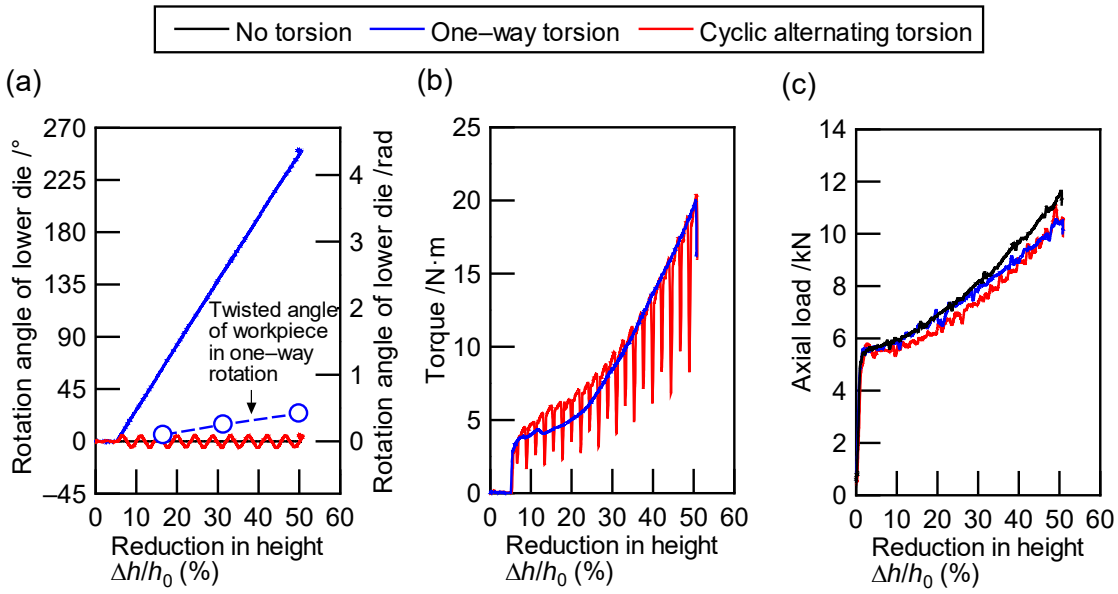

Fig. 5 Experimental results in upsetting of hollow cylinder with ω_r = 0 and 0.5 rpm; (a) rotation angle of lower die, (b) torque, (c) axial load.

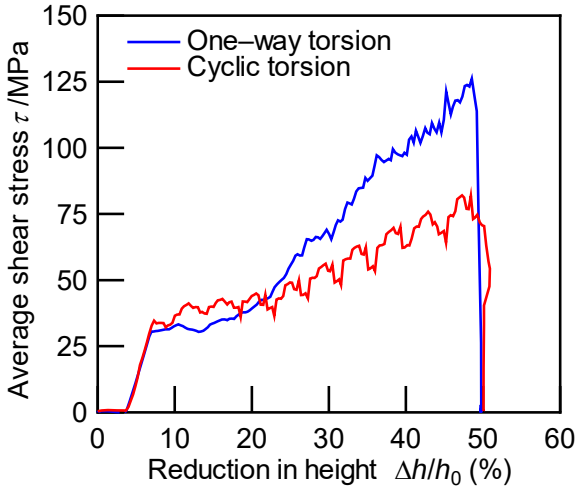

Fig. 6 Estimated average shear stress in upsetting of hollow cylinder with ω_r = 0.5 rpm.

5.2. Deformation of workpiece

Figure 7 shows the experimental results of the inner and outer diameters of the hollow cylinder after upsetting with ω_r = 0.5 rpm. Compared with the diameters of the workpiece after upsetting without torsion, the expansions of the diameters at the top and bottom ends were enhanced by approximately 5% in upsetting with torsion, whereas those at the height center were suppressed by approximately 10%. As the results, the barreling of the workpiece decreased by approximately 10% in upsetting with torsion. This is because the plastic flow of the workpiece increased in the outer lateral direction at the top and bottom ends by combining with torsion, while the plastic flow in the outer lateral direction at the height center was smaller than that without torsion so as to satisfy the constant volume of the workpiece.

Figure 8 shows the experimental results of barreling of the hollow cylinders with h_0 = 5.0–20.0 mm in upsetting. Here the subscripts c and e for the diameters identify height center and end face (top, bottom) of the workpiece, respectively. Some surface scratches on the inner surface of the workpiece are due to tool marks for the initial workpiece. In upsetting of the workpieces with h_0/D_0 = 0.5, barreling was small, and the influence of the combination

of torsion and axial deformation on barreling was also small. In upsetting of the workpieces with $1.0 \leq h_0/D_0 \leq 1.5$, both d_c/d_e and D_c/D_e decreased by approximately 10% due to the combination of torsion and axial deformation. In upsetting of the workpieces with $h_0/D_0 = 2.0$, buckling occurred with/without torsion. In above-mentioned experimental results, the deformation behaviors of the workpiece were the same tendency in one-way and cyclic alternating torsions. **Figure 9** shows the experimental results of barreling of the hollow cylinders with d_0 = 3.0–9.0 mm in upsetting. Both d_c/d_e and D_c/D_e decreased by approximately 10% due to the combination of torsion and axial deformation in upsetting of the workpieces with $d_0/D_0 \leq 0.7$, whereas buckling occurred with/without torsion in upsetting of the workpieces with $d_0/D_0 = 0.9$.

Relationship between the initial shape of the hollow cylinder and the plastic deformation in upsetting with torsion is plotted in **Figure 10**. The combination of torsion and axial deformation could reduce barreling of the workpiece in upsetting with $1.0 < h_0/D_0 \leq 2.0$ and $d_0/D_0 \leq 0.7$, whereas buckling occurred in upsetting with $h_0/D_0 > 2.0$ with/without torsion.

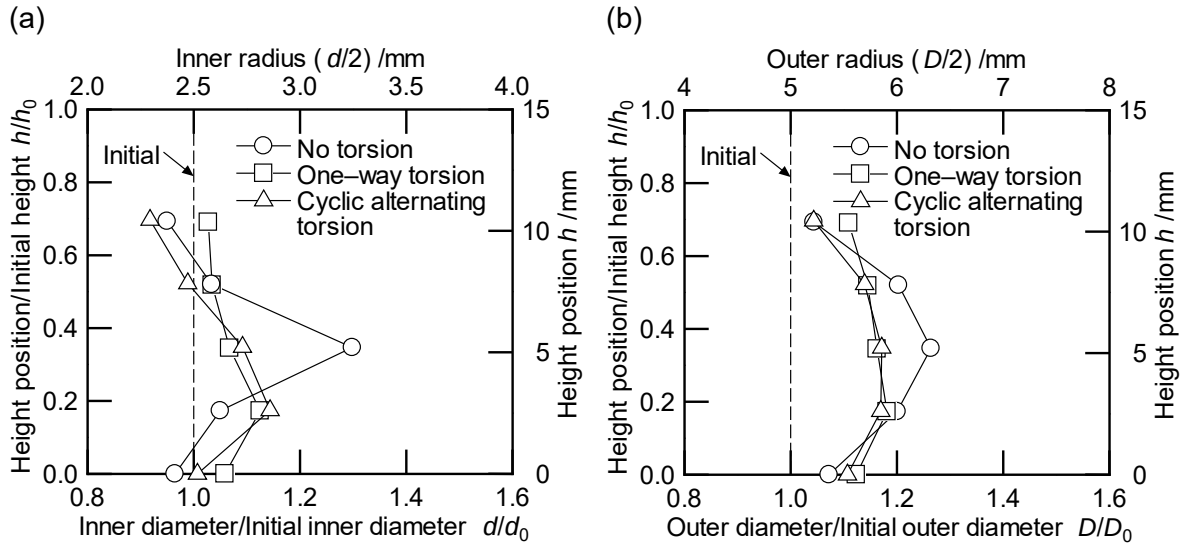

Fig. 7 Experimental results of diameters of hollow cylinder after upsetting with ω_r = 0 and 0.5 rpm ($\Delta h/h_0$ = 30%); (a) inner diameter, (b) outer diameter.

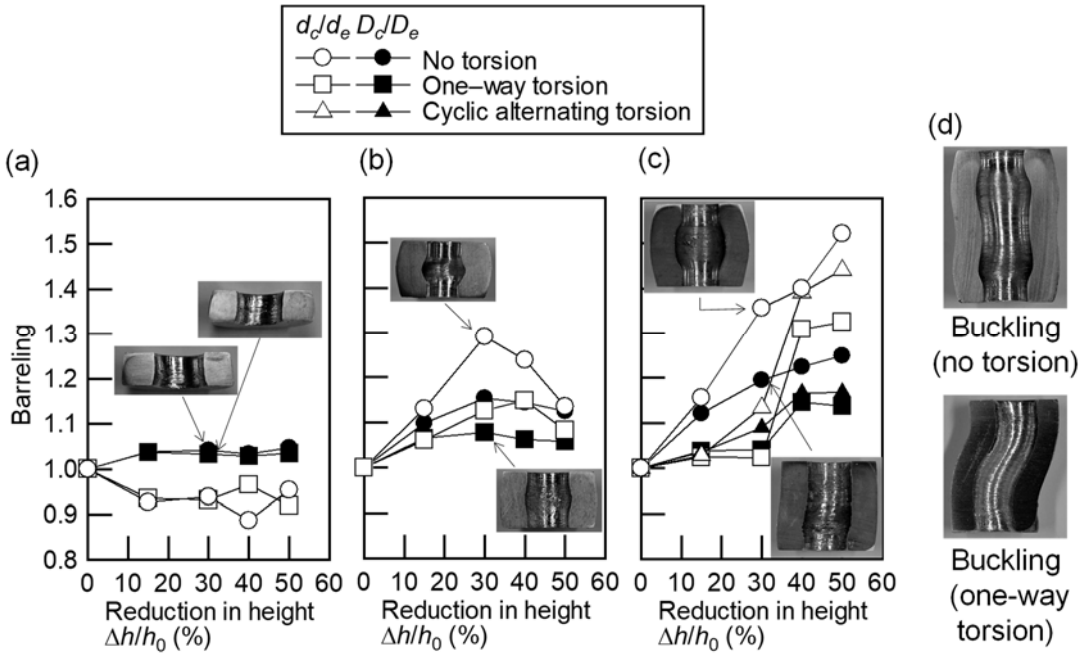

Fig. 8 Experimental results of barreling of hollow cylinder with D_0 = 10.0 mm and d_0 = 5.0 mm in upsetting with ω_r = 0 and 0.5 rpm (subscript c: height center, e: end face (top, bottom)); (a) h_0 = 5.0 mm (h_0/D_0 = 0.5), (b) h_0 = 10.0 mm (h_0/D_0 = 1.0), (c) h_0 = 15.0 mm (h_0/D_0 = 1.5), (d) h_0 = 20.0 mm (h_0/D_0 = 2.0).

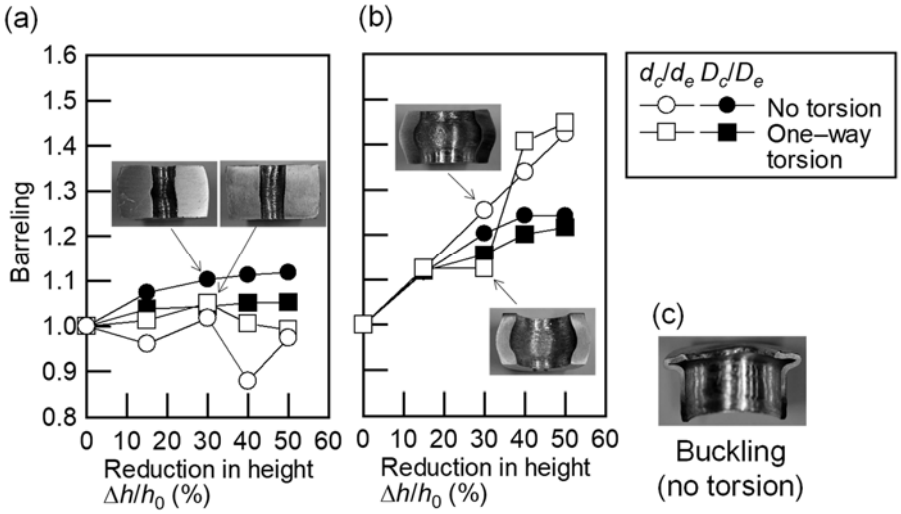

Fig. 9 Experimental results of barreling of hollow cylinder with D_0 = 10.0 mm and h_0 = 10.0 mm in upsetting with ω_r = 0 and 0.5 rpm; (a) d_0 = 3.0 mm (d_0/D_0 = 0.3), (b) d_0 = 7.0 mm (d_0/D_0 = 0.7), (c) d_0 = 9.0 mm (d_0/D_0 = 0.9).

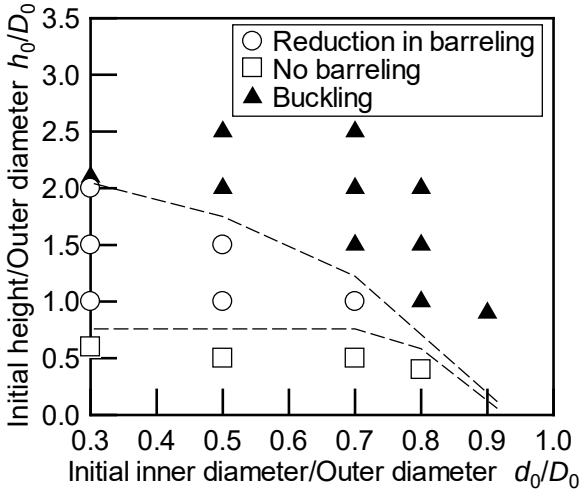

Fig. 10 Relationship between initial shape of hollow cylinder and plastic deformation in upsetting with torsion (ω_r = 0.5 rpm, $\Delta h/h_0$ = 30%).

5.3. Discussions by finite element analysis

5.3.1. Mechanism of enhancement of plastic flow in lateral direction

Since the workpiece in rθ cross-section is deformed in the peripheral direction as well as the lateral direction by combining with torsion during upsetting, the induced strain increases. **Figure 11** shows the finite element analysis results of the radial velocity and the equivalent strain in the rz section of the hollow cylinder in upsetting with one-way torsion. The radial velocity of the workpiece in upsetting with torsion was overall faster than that in upsetting without torsion. The velocity difference between the inner corners of the top and bottom ends and the outer of the height center was slightly small in upsetting with torsion. The increase of the radial velocity led to enhance the plastic flow in the outer lateral direction, while the decrease of the velocity difference led to larger plastic flow at the bottom and top ends than that at the height center. As the results, the strain increased at the inner corners of the top and bottom ends by combining with torsion, so that the strain concentration decreased. On the other hand, strain concentrated at the outer corners of the top and bottom ends and the

inner surface of the height center in upsetting without torsion.

From above analysis results as well as the experimental results described in Section 5.2, the combination of torsion and axial deformation reduces barreling of the workpiece by the increase of the radial velocity of the workpiece, the decreasing of the velocity difference at the inner corners of the top and bottom ends and the decrease of the strain concentration.

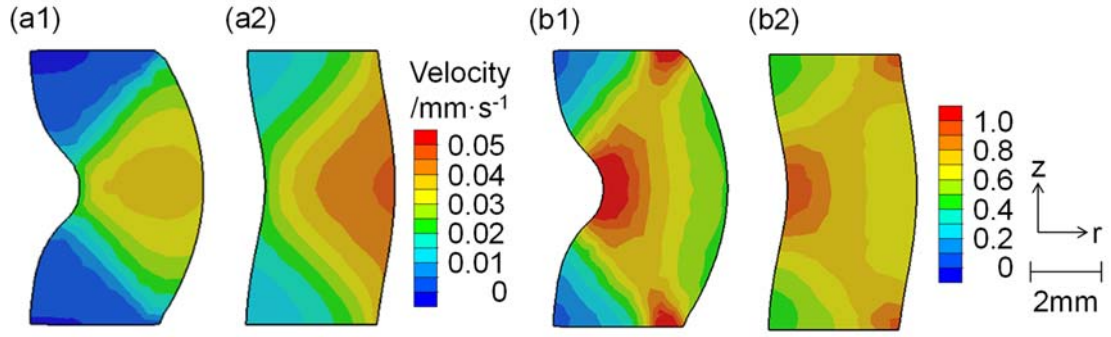

Fig. 11 Finite element analysis results of distributions of equivalent strain and radial velocity in rz section (right half) of hollow cylinder in upsetting ($\Delta h/h_0$ = 50%); (a1) radial velocity in no torsion, (a2) radial velocity in one-way torsion with ω_r = 0.5 rpm, (b1) equivalent strain in no torsion, (b2) equivalent strain in one-way torsion with ω_r = 0.5 rpm.

5.3.2. Equivalent effect in friction reduction

One of conventional approaches to reduce barreling of the hollow cylinder in upsetting is the friction reduction on the die–workpiece interface as mentioned in Section 1. Combination of torsion and axial deformation is a different approach to reduce barreling, however the friction on the die–workpiece interface is required for twist the workpiece by the frictional force. Correlation among the friction on the die–workpiece interface, torsion and barreling is investigated. **Figure 12** shows the finite element analysis results of barreling of the hollow cylinder in upsetting. Here one-way torsion was considered because the maximum reduction in the axial load and the deformation behaviors of the workpiece were the same

tendency in one-way and cyclic alternating torsions as mentioned in Sections 5.1 and 5.2. The workpiece was not twisted under $\mu = 0$ due to the peripheral slip on the die–workpiece interface. The workpiece was twisted under $\mu > 0.5$ without slipping on the die–workpiece interface, however barreling was almost the same with/without torsion because the top and bottom ends of the workpiece were sticked on the die surface. Although both d_c/d_e and D_c/D_e increased with increasing coefficient of friction with/without torsion, these with torsion were lower than those without torsion. For example, D_c/D_e was almost the same in upsetting with torsion under $\mu = 0.3$ and upsetting without torsion under $\mu = 0.03$ in **Figure 12**. This indicates that barreling with torsion under $\mu = 0.3$ is nominally equivalent with barreling without torsion under $\mu = 0.03$ in upsetting of the hollow cylinder.

From above analysis results, from a viewpoint of reduction of barreling in upsetting, the combination of torsion and axial deformation is nominally equivalent to reduce the friction on the die–workpiece interface.

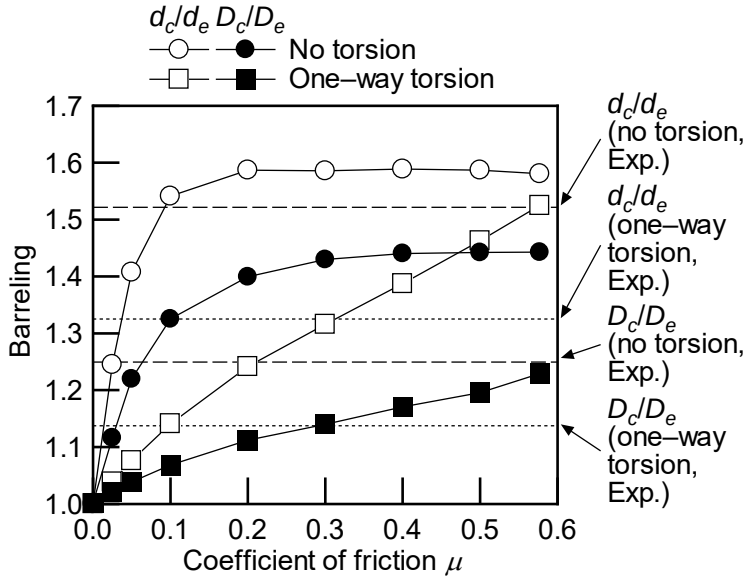

Fig. 12 Finite element analysis results of barreling of hollow cylinder in upsetting with $\omega_r = 0$ and 0.5 rpm under various coefficients of friction ($\Delta h/h_0 = 50\%$).

6. Validity in lateral extrusion with gear shape

6.1 Axial load and torque

Figure 13 shows the photographs of the appearance of the extruded workpiece in lateral extrusion. The distinguished difference of the appearance of (a)–(c) was not seen. The deformation behavior was similar with the behavior predicted by the finite element analysis shown in **Figure 4(c)**. **Figure 14** shows the experimental results of the torque and the axial load in lateral extrusion with ω_r = 0.5 rpm. As predicted in Section 3.3, the workpiece started to be twisted by means of the engagements among the extruded workpiece and the grooves of the punch and rotated die because the torque increased immediately after the die rotation started at s = 0.7 mm. Since the peripheral slips on the punch–workpiece and die–workpiece interfaces did not occur in torsion by the engagement, the workpiece was indicated to be twisted with the die rotation speed ($\omega_r = \omega_t$). Same with upsetting of hollow cylinder in Section 5.1, the torque dropped periodically and momentarily in cyclic alternating torsion because the rotation of the workpiece stopped at the moments of reversal of the die rotation direction. The torque in cyclic alternating torsion was almost the half of the one-way torsion at s < 5.0 mm, however the axial load was almost the same in one-way and cyclic alternating torsions, and the axial load was reduced by maximum 25% in one-way and cyclic alternating torsions in **Figure 14(b)**. The difference of the torque was mainly caused by the difference of the contact length of the side part of the tooth between the die and the extruded workpiece especially at s < 5.0 mm (see Section 6.2). On the other hand, the axially compressed part of the workpiece was twisted almost the same in one-way and cyclic alternating torsions.

From the behaviors of the axial load and torque, the superposition of the axial compression and torsion stresses occurred in lateral extrusion.

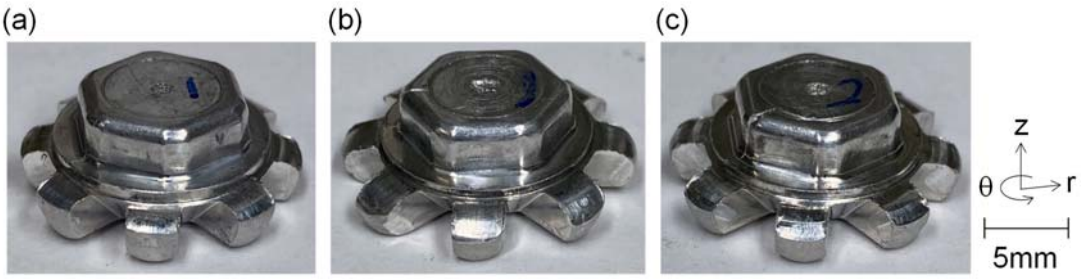

Fig. 13 Photographs of extruded workpiece in lateral extrusion with s = 6.7 mm; (a) no torsion, (b) one-way torsion, (c) cyclic alternating torsion.

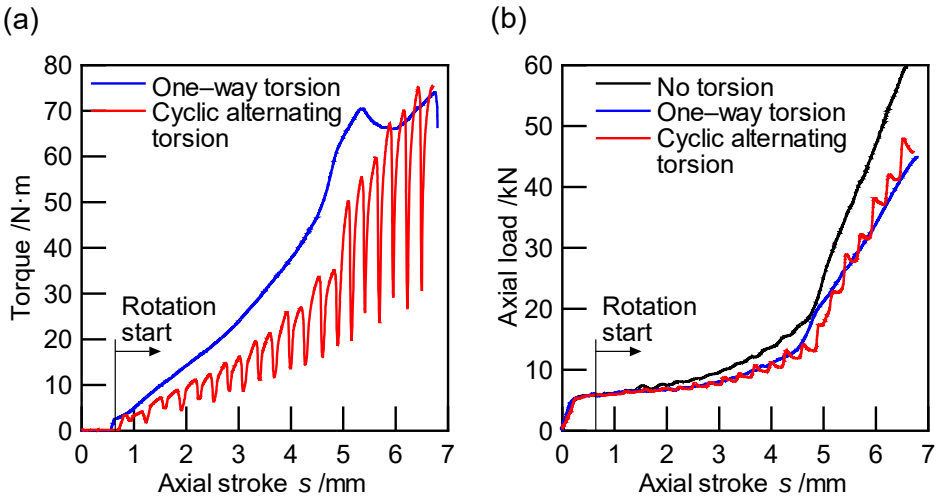

Fig. 14 Experimental results in lateral extrusion with ω_r = 0 and 0.5 rpm; (a) torque, (b) axial load.

6.2. Deformation of workpiece

Figure 15 shows the experimental and finite element analysis results of the inner diameter of the workpiece at the bottom end in lateral extrusion. The outer surface of the workpiece started to be extruded to the tooth cavity at s = 4.8 mm, while the inner surface of the workpiece started to be shrinked. The shrinkage of the inner surface of the workpiece was reduced by approximately 35% in the inner diameter at s = 5.0 mm by combining with torsion due to increase of plastic flow of the workpiece in the outer lateral direction.

The experimental results of the shape of the extruded workpiece at tooth part in lateral extrusion with s = 5.0 mm and 6.7 mm are shown in **Figures 16 and 17**, respectively. The extruded tooth thickness was thinner than the tooth thickness of the die in extrusion with/without torsion. The tooth depth at the center of the tooth thickness direction was approximately 5% and 7% larger extruded at s = 5.0 mm and 6.7 mm in extrusion with torsion, respectively. The $r\theta$ cross-sectional area of the extruded tooth profile increased by approximately 5% and 25% in extrusion with one-way and cyclic alternating torsions, respectively. Plastic flow of the workpiece was enhanced on the rear side surface of die rotation direction in extrusion with one-way torsion, while the workpiece was extruded evenly in the tooth thickness direction in extrusion with cyclic alternating torsion.

Figure 18 shows the finite element analysis results of the deformation behavior of workpiece in $r\theta$ cross-section during one rotation cycle of the die in lateral extrusion with cyclic alternating torsion. The side surface of the extruded tooth part did not contact on the side surface of the tooth of the die in extrusion without torsion because the extruded tooth thickness was thinner than the tooth thickness of the die as mentioned in **Figures 16 and 17**. On the other hand, the side surface of the extruded tooth part contacted on the side surface of the tooth of the die at the rear side of die rotation direction in extrusion with torsion. Due to this, the frictional force was generated on the contact in the tooth depth direction. The side surface of the extruded tooth part slid on the side surface of the tooth of the die in the tooth depth direction by the die rotation. As the result, plastic flow of the workpiece was enhanced on the rear side surface of die rotation direction. Due to the periodic reversal of die rotation direction, the side surface of the extruded tooth part contacted on the side surface of the tooth of the die was changed periodically. The workpiece was extruded evenly in the tooth thickness direction in extrusion with cyclic alternating torsion.

From above results, the die rotation during lateral extrusion with hollow cylinder is

effective to extrude in the outer lateral direction. In addition, the workpiece is extruded evenly in the tooth thickness direction in lateral extrusion with cyclic alternating die rotation.

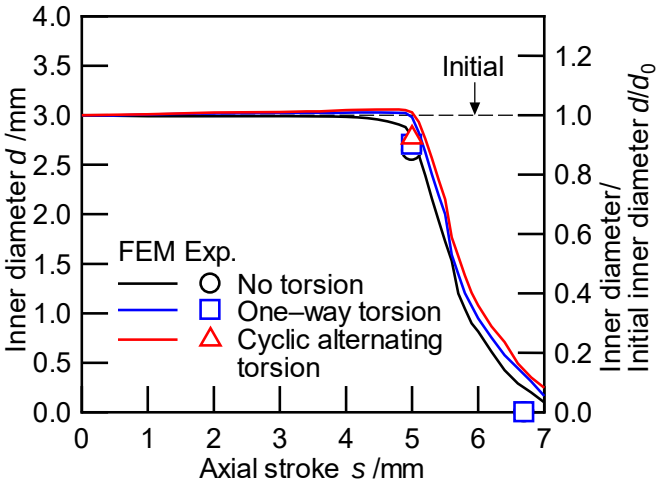

Fig. 15 Experimental and finite element analysis results of inner diameter of workpiece at bottom in lateral extrusion.

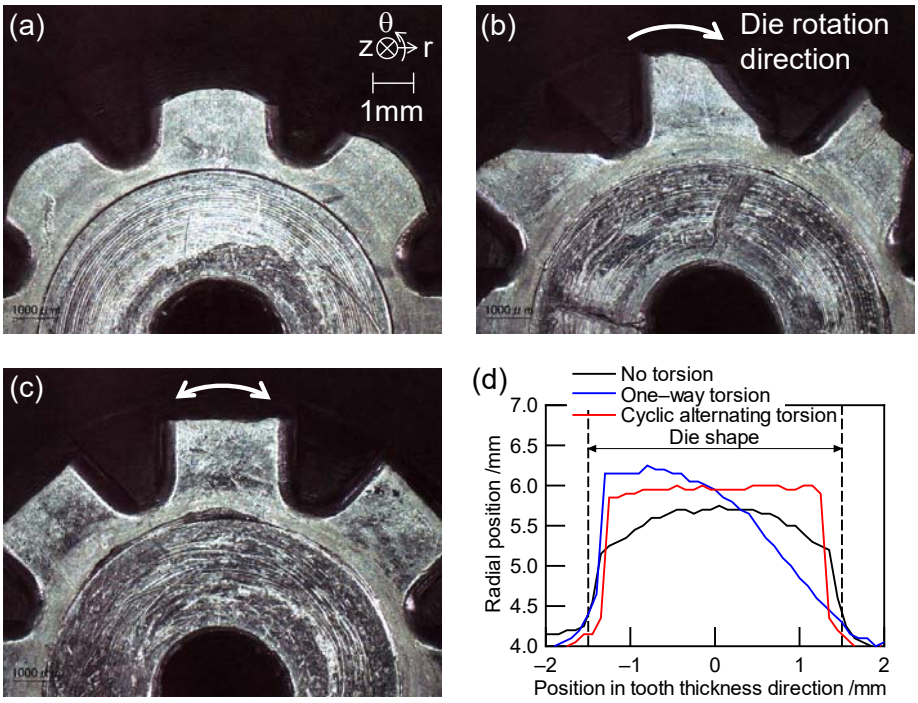

Fig. 16 Experimental results of shape of extruded workpiece at tooth part in lateral extrusion with s = 5.0 mm; (a) no torsion, (b) one-way torsion, (c) cyclic alternating torsion, (d) tooth profiles.

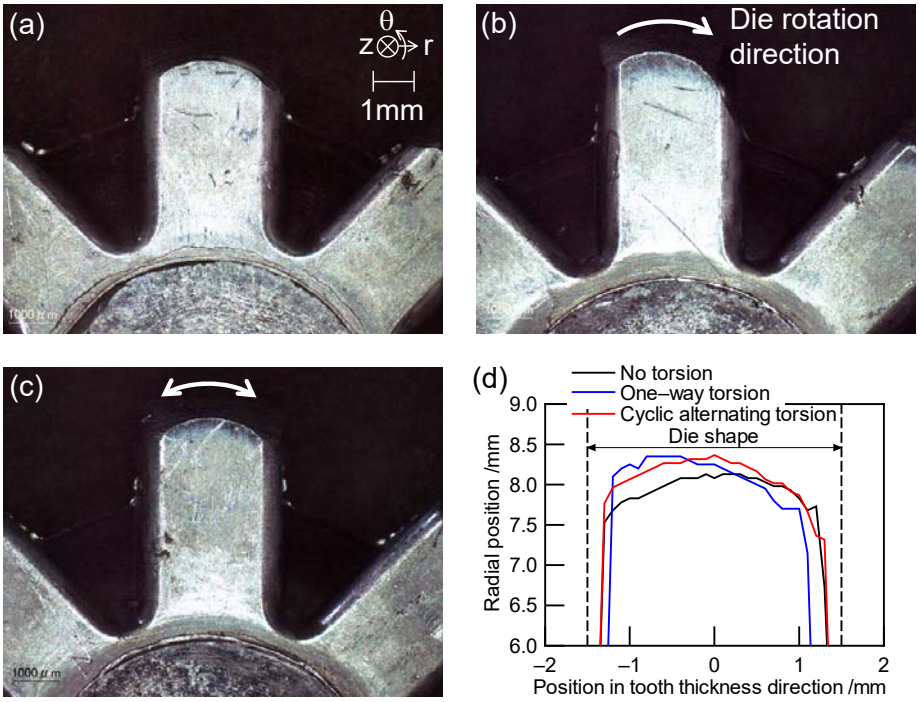

Fig. 17 Experimental results of shape of extruded workpiece at tooth part in lateral extrusion with s = 6.7 mm; (a) no torsion, (b) one-way torsion, (c) cyclic alternating torsion, (d) tooth profiles.

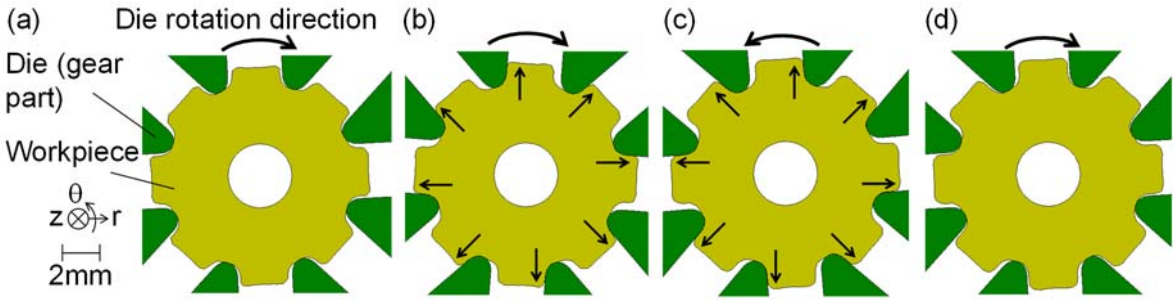

Fig. 18 Finite element analysis results of deformation behavior of workpiece in rθ cross-section during one rotation cycle of die in lateral extrusion with cyclic alternating torsion; (a) rotation angle position: 0°, (b) 5°, (c) -5°, (d) 0°.

6.3. Strain distribution and Vickers hardness

To investigate the change in the hardness of the workpiece by the plastic deformation during lateral extrusion, a JIS C1100 copper drawn bar was used as workpiece in this section due to high work hardening characteristics as a following model of the flow stress:

$$\sigma = 483\varepsilon^{0.42} \quad \text{[MPa]} \tag{6}$$

where σ is flow stress (MPa) and ε is true strain. **Figure 19** shows the finite element analysis results of the equivalent strain of the workpiece at the extruded tooth part. The value and distribution of the equivalent strain are not directly compared in extrusion with/without torsion because the extruded shape of the tooth part is different. However the distribution of the equivalent strain was obviously different. Approximately 2–5 times larger strain was induced to the workpiece at the side of the tooth part in extrusion with torsion, whereas the induced strain at the inner part of the tooth part was almost the same with that of the workpiece extruded without torsion.

The Vickers hardness of the copper workpiece after lateral extrusion is shown in **Figure 20**. Here the hardness was the average value of two-time measurements under an indentation load of 2 N. Compared with the initial workpiece (75 HV0.2), the workpiece was hardened higher than 1.5 times by extrusion with/without torsion. In the workpiece extruded with torsion, the hardness additionally increased near the side surface of the tooth part by approximately 15%.

The amount of strain induced in the lateral extrusion is estimated from the measurement results of the Vickers hardness. Since recrystallization does not occur in cold forming of C1100 copper, the increase in hardness is due to the increase in dislocation density. Relationship between Vickers hardness and flow stress is known as follows:

$$\sigma = \frac{9.8H}{C} \quad \text{[MPa]} \tag{7}$$

where σ is flow stress (MPa), H is Vickers hardness (HV) and C (= 3.0) is constant. Using the

Eqs. (6) and (7), the strain induced at the side of the tooth part was calculated from **Figure 20**. The strain was estimated approximately 1.1 and 0.6 in extrusion with/without torsion, respectively. It is denoted that approximately two times larger strain was induced to the workpiece at the side of the tooth part in extrusion with torsion. This agrees with the finite element analysis results of the strain shown as **Figure 19**.

From above results, the combination of torsion and axial deformation is effective to enhance the strength of the extruded part especially at the side of the tooth part by introducing large strain.

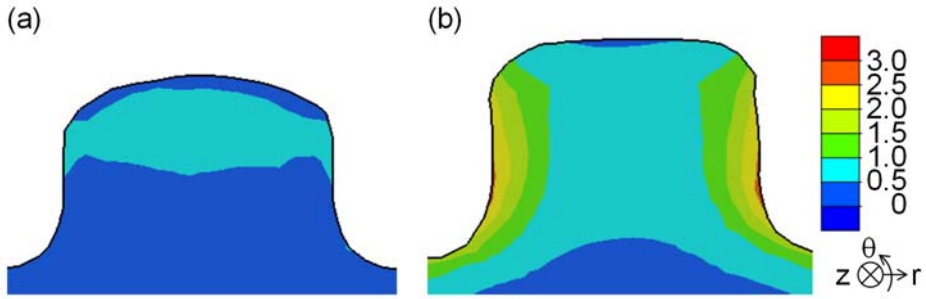

Fig. 19 Finite element analysis results of distribution of equivalent strain in rθ cross-section of C1100 copper workpiece at extruded tooth part in lateral extrusion (s = 5.2 mm); (a) no torsion, (b) cyclic alternating torsion.

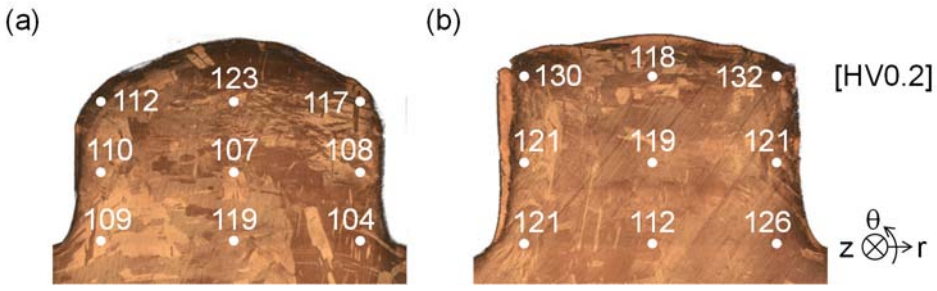

Fig. 20 Experimental results of Vickers hardness of C1100 copper workpiece at extruded tooth part in lateral extrusion (s = 5.2 mm, initial hardness: 75 HV0.2); (a) no torsion, (b) cyclic alternating torsion.

7. Conclusions

In this study, the plastic flow of hollow cylindrical workpiece in upsetting and in lateral extrusion with torsional oscillation was investigated by the experiment and the finite element analysis. The workpiece was compressed axially or extruded laterally between the upper and lower dies. Simultaneously, the workpiece was twisted with the frictional force by rotating the lower die with respect to the axisymmetric axis. The following conclusions were obtained.

(1) Due to superposition of the axial compression and torsion stresses, the axial load was reduced by approximately 10% and 25% in upsetting with twist/compression speed of 6 °/mm and lateral extrusion with twist/compression speed of 30 °/mm, respectively.

(2) In the upsetting of the workpiece with 1.0 < initial height/outer diameter $\leq$ 2.0 and initial inner/outer diameter $\leq$ 0.7, barreling of the workpiece was reduced by approximately 10% under a twist/compression speed of 6 °/mm. This is because the plastic flow of the workpiece increased in the outer lateral direction at the top and bottom ends by combining with torsion, while the plastic flow in the outer lateral direction was small at the height center. Concerning the reduction in barreling of the workpiece, the combination of torsion and axial deformation was nominally equivalent to reduce the friction on the die–workpiece interface.

(3) In the lateral extrusion, the workpiece was twisted by means of the engagements among the extruded workpiece and the grooves of the punch and rotated die. The tooth depth at the center of the tooth thickness direction was approximately 5–7% larger extruded with twist/compression speed of 30 °/mm. The workpiece was extruded evenly in the tooth thickness direction in extrusion with cyclic alternating torsion due to the periodic reversal of die rotation direction.

(4) In the lateral extrusion, the hardness of the JIS C1100 copper workpiece extruded with twist/compression speed of 30 °/mm was approximately 15% higher than the workpiece extruded without torsion near the side surface of the tooth part. This is because larger strain was additionally induced by combining with torsion during extrusion.

Acknowledgements

This study was financially supported in part by the Amada Foundation (AF-2019007-B2) and the Light Metal Educational Foundation, Inc.

References

- Ando, H., 2017, Advantages, features and future prospects of application on servo press. Press Working. 55(11), 18-25.
- Barraclough, D.R., Whittaker, H.J., Nair, K.D., Sellars, C.M., 1973, Effect of specimen geometry on hot torsion test results for solid and tubular specimens. Journal of Testing and Evaluation. 1(3), 220-226. [doi: 10.1520/JTE10007J]
- Bochniak, W., Korbel, A., 2003, KOBO Type Forming: forging of metals under complex conditions of the process. Journal of Materials Processing Technology. 134(1), 120-134. [doi: 10.1016/S0924-0136(02)01033-6]
- Bochniak, W., Korbel, A., Szyndler, R., Hanarz, R., Stalony-Dobrzanski, F., Blaz, L., Snarski, P., 2006, New forging method of bevel gears from structural steel. Journal of Materials Processing Technology. 173(1), 75-83. [doi: 10.1016/j.jmatprotec.2005.09.028]
- Bridgman, P.W., 1943, On torsion combined with compression. Journal of Applied Physics. 14, 273-283. [doi: 10.1063/1.1714987]
- Bridgman P.W., 1964, Studies in large plastic flow and fracture. Harvard University Press. 247-278. [doi: 10.4159/harvard.9780674731349]

- Kim, Y., Park, J., 2003, Upper bound analysis of torsional backward extrusion process. Journal of Materials Processing Technology. 143-144, 735-740. [doi: 10.1016/S0924-0136(03)00385-6]
- Kleiner, M., Geiger, M., Klaus, A, 2003, Manufacturing of lightweight components by metal forming. CIRP Annals – Manufacturing Technology. 52(2), 521-542. [doi: 10.1016/S0007-8506(07)60202-9]
- Korbel, A., Bochniak, W., Ostachowski, P., Błaż, L., 2011, Visco-plastic flow of metal in dynamic conditions of complex strain scheme. Metallurgical and Materials Transactions A. 42, 2881-2897. [doi: 10.1007/s11661-011-0688-x]
- Koprowski, P., Bieda, M., Boczkal, S., Jarzebska, A., Ostachowski, P., Kawalko, J., Czeppe, T., Maziarz, W., Lagoda, M., Sztwiertnia, K., 2018, AA6013 aluminium alloy deformed by forward-backward rotating die (KoBo): Microstructure and mechanical properties control by changing the die oscillation frequency. Journal of Materials Processing Technology. 253, 34-42. [doi: 10.1016/j.jmatprotec.2017.10.043]
- Lee, H.H., Kim, W., Jung, K.C., Seo, S., Lee, J.K., Park, H.L., Park, K.T., Kim, H.S., 2018, Circumferential twisting during route B equal-channel angular pressing. Journal of Materials Processing Technology. 259, 305-311. [doi: 10.1016/j.jmatprotec.2018.05.001]
- Li, Y., Onodera, E., Chiba, A., 2010, Evaluation of friction coefficient by simulation in bulk metal forming process. Metallurgical and Materials Transactions A. 41(1), 224-232. [doi: 10.1007/s11661-009-0066-0]
- Maciejewski, J., Mróz, Z., 2008, An upper-bound analysis of axisymmetric extrusion assisted by cyclic torsion. Journal of Materials Processing Technology. 206(1-3), 333-344. [doi: 10.1016/j.jmatprotec.2007.12.061]
- Matsumoto, R., Kou, J., Utsunomiya, H., 2017, Reduction in axial forging load by low-frequency torsional oscillation in cold upsetting. International Journal of Advanced

Manufacturing Technology. 93(1-4), 933-943. [doi: 10.1007/s00170-017-0553-1]

- Mori, K., Maeno, T., Maki, S., 2007, Mechanism of improvement of formability in pulsating hydroforming of tubes. International Journal of Machine Tools and Manufacture. 47(6), 978-984. [doi: 10.1016/j.ijmachtools.2006.07.006]
- Nadai, A., 1950, Theory of flow and fracture of solids, second ed. McGraw-Hill Book Company, Inc., New York, vol. 1, 347-352.
- Ohga, K., Kondo, K., 1982, Research on precision die forging utilizing divided flow (1st report, theoretical analysis of processes utilizing flow relief-axis and relief-hole). Bulletin of JSME. 25(209), 1828-1835. [doi: 10.1299/jsme1958.25.1828]
- Osakada, K., Mori, K., 1986, A study of buckling in upsetting by use of finite element method. CIRP Annals – Manufacturing Technology. 35(1), 161-164. [doi: 10.1016/S0007-8506(07)61861-7]
- Osakada, K., Wang, X., Hanami, S., 1997, Precision forging of spline by flashless die forging with axially driven die. CIRP Annals – Manufacturing Technology. 46(1), 209-212. [doi: 10.1016/S0007-8506(07)60810-5]
- Politis, D.J., Politis, N.J., Lin, J., Dean T.A., 2018, A review of force reduction methods in precision forging axisymmetric shapes. International Journal of Advanced Manufacturing Technology. 97(5-8), 2809-2833. [doi: 10.1007/s00170-018-2151-2]
- Saunders, I., Nutting, J., 1984, Deformation of metals to high strains using combination of torsion and compression, Metal Science. 18(12), 571-576. [doi: 10.1179/030634584790419629]
- Tatematsu, Y., Morimoto, M., Kitamura, K., 2018, Experiment and FE analysis of compression of thick ring filled with oil. Key Engineering Materials. 767, 141-148. [doi: 10.4028/www.scientific.net/KEM.767.141]
- Tekkaya, A.E., Becker, C., Ortelt, T., Grzancic, G., 2015, Utilizing stress superposition in

metal forming. Proceedings of the 7th JSTP International Seminar on Precision Forging 1-6.

- Verleysen, P., Lanjewar, H., 2020, Dynamic high pressure torsion: A novel technique for dynamic severe plastic deformation. Journal of Materials Processing Technology. 276, 116393. [doi: 10.1016/j.jmatprotec.2019.116393]
- Wang, Q., Zhang, Z., Yu, J., Xue, Y., 2017, A novel backward extrusion process through rotating die and open punch. Procedia Engineering. 207, 383-388. [doi: 10.1016/j.proeng.2017.10.792]
- Weglarczyk, S., Madej, L., Hanarz, R., Bochniak, W., Szyndler, R., Korbel, A., 2008, Validation of the numerical simulation of forging of gear-wheel in the reversible rotating die. Steel research international. 79, Special Edition, 789-796.
- Weiss, A., Liewald, M., Weiss, A., Missal, N., 2018, Manufacturing of face gear – a new production method by means of determined material pre-distribution. Procedia Manufacturing. 15, 511-518. [doi: 10.1016/j.promfg.2018.07.261]